Article:
Devine, M., Hornsby, D., O Brádaigh, C.M. et al. (2026) Role of fibre sizing in interfacial relaxation, water uptake and fatigue properties of acrylic-matrix composites. Polymer Composites. ISSN: 0272-8397

https://doi.org/10.1002/pc.71367

Polymer Composites

WILEY | spe INSPIRING PLASTICS PROFESSIONALS

RESEARCH ARTICLE OPEN ACCESS

Role of Fiber Sizing in Interfacial Relaxation, Water Uptake and Fatigue Properties of Acrylic-Matrix Composites

Machar Devine | Duncan Hornsby | Conchúr M. Ó Brádaigh | Dipa Ray

School of Engineering, Institute for Materials and Processes, The University of Edinburgh, Edinburgh, Scotland, UK

Correspondence: Dipa Ray (dipa.roy@ed.ac.uk)

Received: 5 May 2026 | **Revised:** 15 June 2026 | **Accepted:** 17 June 2026

Keywords: fatigue | fiber-matrix interface | glass fiber reinforcement | hydrothermal aging | thermoplastic composites | tidal energy | wind energy

ABSTRACT

Fiber-reinforced infusible acrylic monomer resins are of interest as recyclable alternatives to epoxy and other thermoset resin composites, but the novelty of these resins causes published studies on acrylic-matrix composites to often rely on multi-compatible or other non-tailored fiber sizing agents. It has been suggested that improvements to the mechanical properties, water absorption, and fatigue behavior may be gained with a sizing agent tailored specifically to acrylic resins. In this study, glass-fiber/acrylic composites, treated with either a multi-compatible sizing agent or an acrylic-tailored sizing agent, are compared. Their retention of mechanical and fatigue properties after saturation with seawater, and the degree of interfacial relaxation during repeated absorption–desorption cycles, are used to explore the role of the sizing in water absorption. These results, supported by fractography, suggest that the tailored sizing agent did not significantly improve the water absorption behavior of the materials. The fatigue performance of the composites with the different sizing agents was similar. The static mechanical properties which are dominated by the fiber-matrix interface, such as transverse tensile and flexural strengths, showed that the multi-compatible sizing agent performed better than the tailored acrylic sizing agent.

1 | Introduction

The use of fiber reinforced polymer composites (FRPs) in offshore renewable energy is expected to increase in the coming years due to growth in the offshore wind and tidal energy sectors. The most common polymer matrices used in such composites are thermosets such as epoxy, but they are unable to be re-shaped or recycled once they have been cured due to their crosslinked structure and are typically disposed of in landfill or via incineration [1]. Thermoplastics, in contrast, liquefy upon heating and dissolve in solvents, so they can be reused and recycled. Liquid acrylic monomeric resins (Elium) from Arkema are currently the only commercially available, infusible thermoplastic resins which polymerize at room temperature and can therefore be considered a "drop-in" replacement for epoxy resins. The promising mechanical properties of these resins have already been demonstrated in the literature [2–7], and their applicability to large structures has been demonstrated through the manufacture of 9 and 62 m long wind turbine blades [8, 9].

Commercially available components such as reinforcements and adhesives are typically designed for compatibility with established resin systems such as epoxy or polyester. This can pose a challenge for novel resin systems such as liquid acrylic monomer resins, as incompatibilities can cause reductions in structural performance. An example of this is given by an acrylic-matrix tidal turbine blade manufactured by Murray et al. [10], which failed prematurely due to an incompatibility between the acrylic resin and the adhesive and foam filler, which were designed to be compatible with epoxy resins.

Similarly, reinforcement fibers are rarely treated with acrylic-specific sizing agents—mixtures of a film former and a coupling agent, among other components, which are applied to the fiber surface for protection and to promote bonding with

Highlights

- Multi-compatible and acrylic-specific sizing agents are compared in acrylic composites.
- Acrylic-specific sizing shows no consistent mechanical or fatigue advantage.
- Both sizings exhibit similar interfacial degradation in hydrothermal aging.
- Readily available reinforcements are suitable for recyclable blade structures.

the matrix [11]. Instead, multi-compatible sizing agents are often used, provided that they are compatible with polyester or vinylester resins. These can have good compatibility with acrylic resins [3], and Arkema itself recommends using a polyester- or vinylester-compatible sizing agent rather than a specialized sizing [12]. It has been shown that a tailored sizing agent improves the dry mechanical properties of a composite, and the retention of these properties upon saturation with water, compared to an incompatible sizing agent [13, 14], but it has been further speculated that a tailored sizing agent would improve the mechanical and fatigue properties, as well as durability in aqueous environments, over a multi-compatible sizing agent [1, 7].

Yet contradictory information exists in the literature regarding the necessity of these acrylic-tailored sizing agents. On the one hand, some researchers suggest that acrylic-tailored sizing agents improve interfacial strength, fatigue life, and water absorption over multi-compatible sizing agents [1, 7, 14, 15], but on the other hand, microbond testing has found no difference in performance [16]. In one study, the presence of a multi-compatible sizing agent produced no improvement in interfacial shear strength between the acrylic matrix and glass fiber, compared to de-sized fibers [17]. These publications have various complications in their comparisons, including chemical incompatibilities with the multi-compatible sizing agent [15, 17], comparing coupons with different layups [1, 7], the use of acrylic latexes instead of Elium resin [14], and the addition of paraffin wax to the resin [16]. Conclusions about GF/acrylic composites are therefore difficult to draw from these studies.

Other studies investigate the effect of the sizing agent on the water absorption behavior of glass–fiber reinforced composites with different matrices. Tsenoglou et al. [13] studied the quality of an interfacial bond via repeated absorption–desorption cycles in GF/polyester short beam shear coupons. The reinforcement fibers were treated with one of: a silane coupling agent, an incompatible polymer (PDMS) or no coating. The ILSS was significantly affected by the fiber treatment, with the clean, PDMS-coated and silane-treated coupons having strengths of 14.1, 7.34, and 29.6 MPa, respectively. The composite coupons, along with neat resin coupons, were then immersed in distilled water and their masses were monitored to allow their diffusion coefficients to be calculated and compared. The silane surface treatment resulted in both slower diffusion and a lower maximum water content than clean or PDMS-coated fibers. The coupons were then dried for 30 h under vacuum, and the absorption–desorption cycle was repeated a further three times. By assuming that diffusion occurred via a free-volume mechanism, Tsenoglou et al. [13] compared the degree of interfacial loosening between the fiber treatments. For clean and silane-treated fibers, interfacial loosening increased with subsequent absorption–desorption cycles, although the silane treatment resulted in a lowered interfacial free volume fraction. In PDMS-coated fibers, interfacial loosening was not observed which was attributed to swelling of the coating. This study not only shows the importance of a silane coupling agent for interfacial strength, but also how the compatibility of other components of the sizing agent with the polymer may affect strength and absorption behavior [11].

Thomason [18] conducted a study on the influence of fiber sizing, resin and void content on the absorption behavior and ILSS of GF/epoxy composites. The fiber surface coating was found to have a much smaller effect on absorption behavior than the void content and matrix resin type, although it did affect the ILSS. It is suggested by the authors that this is due to most of the tested reinforcements being sold as "epoxy-compatible." Indeed, the only reinforcement which performed poorly in water absorption was the only one not marketed as "epoxy-compatible."

There therefore remains significant confusion in the literature regarding the role of specialized sizing agents in acrylic-matrix composites, and further research is essential to better understand if these specialized reinforcements provide any benefits over their multi-compatible counterparts. The sizing effects on the mechanical and fatigue properties of the composite are of interest across a range of industries, but the effect on interfacial relaxation, water absorption, and saturated mechanical properties will be of particular interest to the tidal energy sector.

Previous work by the authors of this paper to characterize the static [3] and fatigue [19] properties of dry and water-saturated GF/acrylic with a multi-compatible sizing agent provides an opportunity to create a comparison with an acrylic-tailored glass fiber reinforcement [20]. The current work therefore explores the effect of sizing agent in GF/acrylic in three ways. The effect of the sizing agent on water diffusion, interfacial relaxation, water absorption–desorption behavior, and resistance to absorption-induced damage is explored via the method introduced by Tsenoglou et al. [13]. Repeated absorption–desorption cycles are applied to multi-compatible and acrylic-specific GF/acrylic composites, as well as unreinforced acrylic resin, to compare the degree of interfacial loosening between the sizing agents. The effects of the tailored sizing agent on the quasi-static mechanical properties of dry and saturated GF/acrylic composites are measured and compared with previous results from coupons made with a multi-compatible glass fiber [3]. Fractography is then used to analyze the damage and failure mechanisms of the coupons. Finally, the S–N curves of dry and saturated GF/acrylic coupons with an acrylic-specific sizing agent are compared with available data using a multi-compatible sizing agent [19] to understand the effects of the sizing agent on fatigue behavior.

TABLE 1 | A comparison of the fabric and fiber properties of GF1-MCS and GF2-AS.

	GF1-MCS	GF2-AS
Fiber type	E-glass	E-glass
Nominal weight (g/m^2)	646	1200
Fiber diameter (μm)	13	16
Tow size (TEX)	1200	2400
Nominal ply thickness (mm)	0.5	1
Sizing agent	Multi-compatible	Acrylic-specific
Image	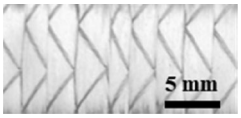	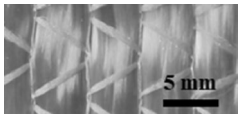

2 | Experimental

2.1 | Material Details

Two unidirectional glass fiber reinforcements treated with different sizing agents were investigated. Although the exact chemical makeup of these sizing agents is known solely by the manufacturers, the first was treated with a multi-compatible sizing agent, supplied by Ahlstrom-Munksjö and suitable for use with unsaturated polyester, vinyl ester, and epoxy resins, and will be referred to as GF1-MCS. This fabric was previously shown to have good compatibility with acrylic resin [2, 3], most likely due to its compatibility with polyester and vinyl ester which, like acrylic, undergo free radical polymerization. The second fabric was treated with an acrylic-specific sizing agent so will be referred to as GF2-AS. GF2-AS, along with its specialized sizing agent, was developed and supplied by Johns Manville. The reinforcements are compared in Table 1, where it should be noted that the areal weight of GF2-AS was approximately twice that of GF1-MCS, and that GF2-AS has a 23% greater fiber diameter. The higher fiber diameter and tow size of GF2-AS result in lower expected costs—both of the fabric itself and in the manufacture of the large composite parts, as fewer plies result in lower handling costs—but also differences in mechanical properties as discussed in Section 3.3.

2.2 | Laminate Manufacture

Flat GF/acrylic laminates were manufactured via a standard vacuum infusion method. Elium 188 O acrylic resin was mixed in a 100:3 weight ratio with a benzoyl peroxide initiator (BP-50-FT, United Initiators), infused into the reinforcement and then allowed to polymerize at room temperature for 24 h before demolding. Test coupons were then cut using a diamond-tipped wet saw to the dimensions specified by the relevant ASTM standards. Both GF1-MCS and GF2-AS were used to manufacture coupons for the measurement of water diffusion, but only GF2-AS was used for mechanical testing and fatigue coupons since GF1-MCS had been characterized in previous studies [3, 19].

In addition, coupons of unreinforced acrylic polymer were manufactured via casting of Elium 188 O resin. Resin was poured into polypropylene molds to approximately the same thickness as the reinforced water diffusion coupons. The mold was sealed with vacuum bagging film, and the resin polymerized at room temperature for 24 h before cutting to 4 mm × 8 mm × 24 mm with a diamond-tipped wet saw.

2.3 | Fiber and Void Volume Fractions

Fiber (FVF), matrix, and void volume fractions were determined using a burn-off method (ASTM D3171, Procedure G). Values for the fiber, matrix, and composite densities were measured via the displacement of water (ASTM D792).

2.4 | Water Immersion

All mechanical and fatigue tests were conducted on both dry and aged coupons. Aging was conducted by immersing the coupons in natural seawater, collected from the Firth of Forth, Edinburgh, Scotland, at 50°C for 3 months to replicate the conditions previously applied to GF1-MCS/acrylic [3, 19]. Aged mechanical test coupons were not subject to any drying stages and were simply wiped to remove surface water before testing.

2.5 | Repeated Absorption–Desorption Cycles

Water diffusion coupons were cut to the suggested dimensions for short beam strength coupons (4 mm × 8 mm × 24 mm) according to ASTM D2344. As noted by Tsenoglou et al. [13], this is not the geometry recommended to determine the through-thickness diffusion coefficient by ASTM standard D5229/D5229M-20, which requires a width-to-thickness ratio of $w/h \geq 100$ to minimize edge effects. Instead, an overall "effective" diffusion coefficient was experimentally determined, where water diffusion through the sides of the specimen was allowed, as the differences in water absorption between composites made with each reinforcement were the critical interest.

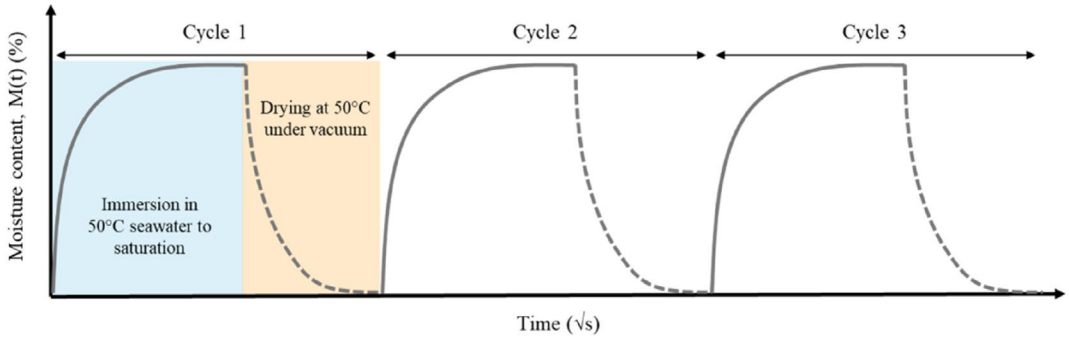

FIGURE 1 | An illustration of the three absorption–desorption cycles applied to the coupons.

All specimens were dried in an oven at 50°C for 24 h and then hydrothermally aged by immersion in seawater at 50°C. As the coupons absorbed water, their increase in mass was periodically recorded using an analytical balance until saturation was reached. The percentage weight gain or moisture content, $M(t)$, at a given time t was calculated from Equation (1), where W_i is the mass of the specimen at time t and W_b is the mass of the specimen when dry.

$$M(t) = \frac{(W_i - W_b)}{W_b} \times 100 \tag{1}$$

After saturation, all the coupons were dried in an oven under vacuum at 50°C and their weight was again periodically measured until no mass change was observed and the coupons were fully dried. Figure 1 shows the process of a single absorption cycle, carried out until saturation is reached, and the subsequent drying cycle. To understand the effects of repeated wet–dry cycles, this process was repeated for a second and third absorption/drying cycle.

The effective diffusion coefficients were calculated for each absorption cycle from Equation (2) (adapted from ASTM D5229-20) where M_m is the moisture equilibrium value, D_e is the effective diffusion coefficient, and h is the thickness of the specimen.

$$M(t) = M_m\left(1 - \exp\left[-7.3\left(\frac{D_e t}{h^2}\right)^{0.75}\right]\right) \tag{2}$$

Equation (2) was fitted to the experimental data, and values for D_e and M_m were extracted from the fitted curve.

2.6 | Calculation of Relaxation of the Fiber–Matrix Interface

Repeatedly cycling between wet and dry cycles is expected to cause loosening or *relaxation* of the fiber–matrix interface—that is, a detachment of the fiber–matrix bond resulting in an increase in the interfacial free-volume fraction, f_i. It is well established in the literature that poor interfacial bonding, resulting in a large f_i, increases the diffusion coefficient of water in a composite. Enhancing the wetting and bonding between fiber and the matrix, as well as resistance to interfacial relaxation, helps mitigate this issue by restricting water or moisture diffusion pathways, thereby reducing water wicking and subsequent hydrothermal degradation in composite materials.

Tsenoglou et al. [13] present a method for quantifying f_i using the diffusion coefficient of water in the composite compared to that in neat resin, with the assumption that diffusion occurs through the free volume of the polymer and composite. The method is explained in full by Tsenoglou et al. [13], however two key equations are presented below. In Equation (3), the initial interfacial free volume fraction f_{i0} is defined as the ratio of the initial void fraction V_i to the fiber volume fraction V_F, where it is assumed by Tsenoglou et al. [13] that the initial void content is due to imperfect interfacial bonding. A more suitable sizing agent is therefore assumed to reduce f_{i0}.

$$f_{i0} = \frac{V_i}{V_i + V_F} \approx \frac{V_i}{V_F} \tag{3}$$

In Equation (4), the interfacial free volume fraction during each absorption cycle (f_i) is calculated from the molecular free volume fraction of the polymer (f_P), the fiber volume fraction (V_F), and the composite and polymer diffusion coefficients (D_e and D_P, respectively).

$$f_i = \frac{f_P}{V_F}\left[\frac{1}{1 - f_P \ln\left(\frac{D_e}{D_P}\right)} - (1 - V_F)\right] \tag{4}$$

In the present work, f_i is calculated using Equation (4) after each absorption cycle. The values of V_F, D_P, and D are determined experimentally, and the value for f_P was taken to be the same as that provided by Tsenoglou et al. [13] at $f_P = 0.08$.

2.7 | Quasi-Static Mechanical Testing

Longitudinal and transverse tensile testing was performed in accordance with ASTM D3039M-17 for both the dry and aged specimens. Coupons of dimensions 250 mm × 15 mm × 2 mm for 0° fibers and 175 mm × 25 mm × 2 mm for 90° fibers were tested in tension until fracture using an Instron universal testing machine (Instron 3369) equipped with a 50 kN load cell. All samples were speckled with spray paint and strain was measured using an Imetrum UVX video extensometry system.

The longitudinal and transverse flexural moduli and strengths were experimentally determined via a 3-point flexural test as per ASTM standard D7264M-21. A span-to-thickness ratio of 32:1 was used as per the standard's recommendations. This gave specimen dimensions of 154 mm × 13 mm × 4 mm and a span of

128 mm. A 3-point bending fixture was attached to the Instron testing machine and fitted with a 10 kN load cell.

2.8 | Fatigue Testing

Coupons were tested in tension–tension fatigue using an Instron 8802 servohydraulic fatigue testing system equipped with a 250 kN load cell and grip pressure of 60 bar, using a testing frequency of 5 Hz and an R-ratio of 0.1. Fatigue coupons were tabbed with GF/epoxy PCB board bonded with cyanoacrylate adhesive. Laminates were specifically manufactured for fatigue testing, and so to ensure quality, separate UTS measurements from the quasi-static testing were taken for the dry and aged GF2-AS/acrylic using an average of three tensile tests. These values were used when deciding the applied stress levels.

Given the expected differences between the mechanical properties of the fabrics, the stress levels (the maximum stress applied during a load cycle) for GF2-AS/acrylic were set at 80%, 60%, and 40% of the UTS of GF2-AS/acrylic, as well as 80%, 60%, and 40% of the UTS of GF1-MCS/acrylic, resulting in six stress levels. A single additional test was performed at 30% of the UTS of dry and aged GF2-AS/acrylic to investigate higher-cycle fatigue and the existence of a fatigue limit. The applied stresses are summarized in Table 2. Coupons were randomly assigned to an aging condition and stress level after cutting.

To keep the aged coupons wet during testing, they were covered in a wet cloth and wrapped in a plastic vacuum bagging (Figure 2).

The Basquin relation (Equation 5) relates stress (S) to the number of cycles to failure (N) with two coefficients, A and b. The Basquin relation may alternatively be expressed as Equation (6) in which $a = 10^A$. Although S may be defined in several ways, in the present work it refers to the maximum stress applied in a load cycle. This relationship applies to the portion of the S–N curve in which progressive damage occurs, and only above the fatigue limit of the material (Figure 3) [21, 22], hence Equation (5) was fitted to experimental data for $S \leq 80\%$ of UTS using linear regression.

$$\log_{10} N = \log_{10} A + b \cdot \log_{10} S \tag{5}$$

$$N = a \cdot S^b \tag{6}$$

TABLE 2 | The stress levels used to test dry and aged GF2-AS/acrylic coupons.

Dry		Aged	
Stress (MPa)	**%UTS**	**Stress (MPa)**	**%UTS**
642	90	520	90
568	80	462	80
481	68	428	74
426	60	347	60
321	45	286	49
284	40	231	40
213	30	173	30

2.9 | Scanning Electron Microscopy

Scanning electron microscopy (SEM) was used to assess the tensile failure and void contents of the composite laminates. Fragments of fractured dry and aged 0° tensile specimens were inspected, followed by cross-sectional imaging of both GF1-MCS/acrylic and GF2-AS/acrylic. The cross sections were cast in epoxy and polished. The samples were coated with 40 nm of gold to enhance the surface conductivity. A 15 kV JEOL JSM-IT100 series SEM instrument was used for image acquisition.

3 | Results and Discussion

3.1 | Fiber and Void Volume Fractions

The average fiber and void volume fractions are presented in Table 3.

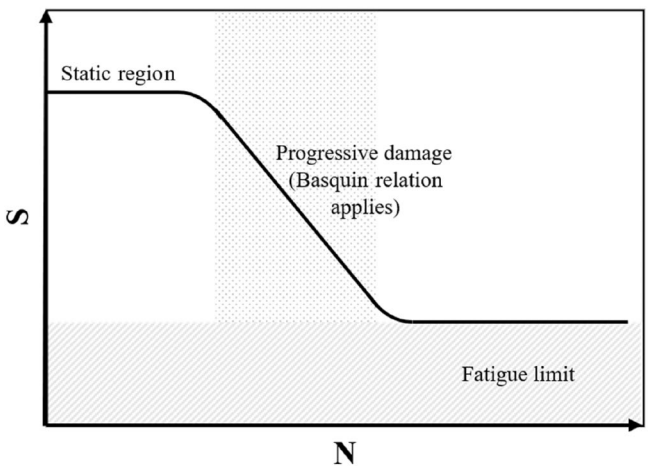

FIGURE 3 | The structure of an S–N curve, adapted from Talreja [21]. Equation (5) was fit to the data in the region of progressive damage.

FIGURE 2 | Aged coupons were kept wet during testing by covering with a saturated cloth and plastic wrap.

3.2 | Sizing Agent Effects on Water Absorption

3.2.1 | Absorption-Desorption Cycles

The diffusion curves, fitted according to Equation (2), for all three absorption cycles of the neat resin and both composites are presented in Figure 4. The resulting values for the diffusion coefficient and maximum water uptake are given in Table 4. There is a general trend of increasing diffusion coefficient and water uptake with subsequent absorption cycles. The diffusion coefficient of the neat resin was higher than that of the composites in the first absorption cycle, but during subsequent cycles the diffusion coefficients of the composites exceeded the neat resin. The value of M_m in the neat resin remained higher than that of the composites, reaching 1.51% during the third absorption cycle versus 0.42% in GF1-MCS/acrylic and 0.83% in GF2-AS/acrylic. The majority of absorbed water therefore resides in the matrix, in contrast with Tsenoglou et al. [13] but in agreement with the work by Davies et al. comparing GF/acrylic composites with unreinforced acrylic [1]. During subsequent cycles, the loosened interface in the composites (discussed in Section 3.2.3) creates a wicking effect and increases the diffusion coefficient [23, 24].

TABLE 3 | Average fiber and void volume fractions of the manufactured laminates, ± one standard deviation. The values for GF1-MCS/acrylic fatigue coupons are from [19].

Laminate	Nominal thickness (mm)	FVF (%)	Void volume fraction (%)
Tensile (GF2-AS)	2	48.2 ± 1.0	0.42 ± 0.28
Flexural and SBS (GF2-AS)	4	54.7 ± 0.3	1.31 ± 0.08
Fatigue (GF2-AS)	2	49.9 ± 1.3	2.4 ± 0.3
Fatigue (GF1-MCS)	1.5	53.5 ± 0.8	1.9 ± 0.4
Diffusion (GF1-MCS)	4	52.9 ± 0.3	0.22 ± 0.16
Diffusion (GF2-AS)	4	51.3 ± 0.2	1.37 ± 0.26

3.2.2 | The Effects of Voids

The higher initial diffusion coefficient and maximum water content observed in GF2-AS/acrylic compared to GF1-MCS/acrylic may be explained by a higher void content in the former. Matrix burn-off tests gave 0.22% and 1.37% void contents for the GF1-MCS and GF2-AS laminates respectively (Table 3), and SEM was also used to validate the void content results. Figure 5 shows cross-sectional SEM images of the GF1-MCS and GF2-AS composites, which were cast in epoxy and polished.

Figure 5a,b shows no visible voids in the GF1-MCS composite. Multiple cross-sections were studied from various locations throughout the laminate, and no voids were found. In contrast, Figure 5c,d shows many intra and inter-tow voids within the GF2-AS composite laminate, agreeing with the results of the burn-off test.

A greater number of voids in the composite results in more volume for the water to occupy and use as ingress routes into the center of the material. This explains the higher maximum water uptake and diffusion values seen by GF2-AS/acrylic during the first cycle. Differences in the fabric properties shown in Table 1, such as the tow size, fiber diameter, and aerial weight, could affect

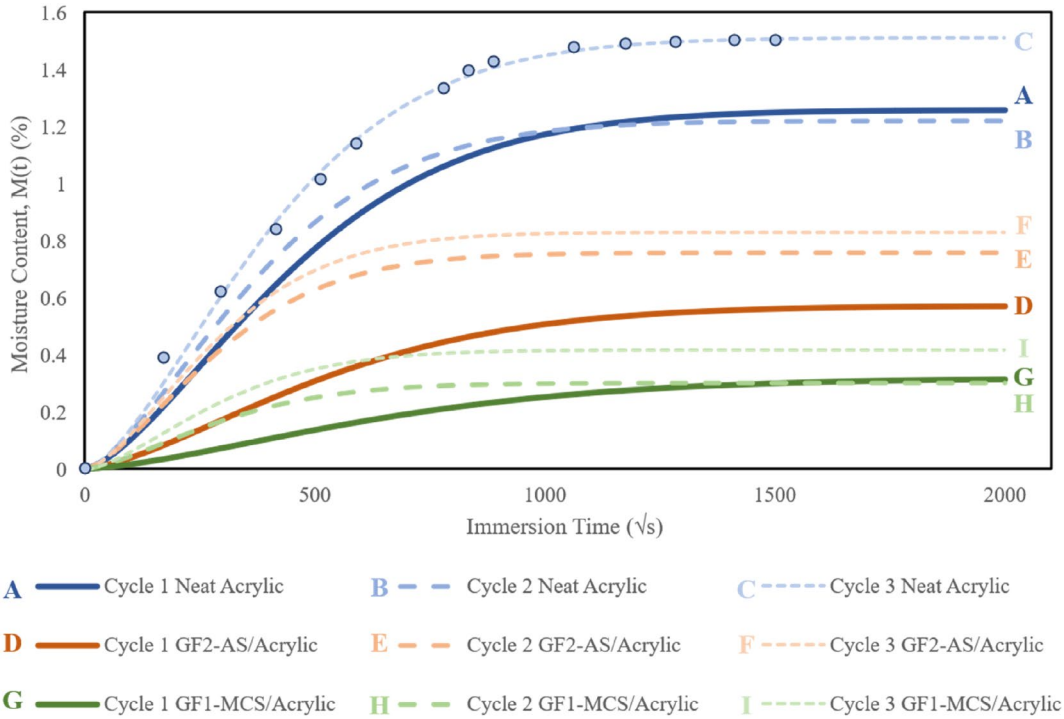

FIGURE 4 | The fitted diffusion curves (using Equation 2) plotted against the square root of time. All three absorption cycles of neat acrylic resin (blue, A–C), GF2-AS/acrylic (orange, D–F) and GF1-MCS/acrylic (green, G–I) are presented. For clarity, only the experimental data from the third neat acrylic cycle (C) has been included as blue circles. All experimental data is available in Figure S1.

TABLE 4 | Effective diffusion coefficients for materials tested under 3 immersion cycles at 50°C.

	Cycle	GF1-MCS/acrylic	GF2-AS/acrylic	Unreinforced acrylic
Diffusion coefficient, D_e ($\times 10^{-12}$ m^2 s^{-1})	Cycle 1	1.77	2.69	5.54
	Cycle 2	8.25	8.09	7.84
	Cycle 3	8.65	8.52	7.00
Equilibrium water content, M_m	Cycle 1	0.32%	0.57%	1.26%
	Cycle 2	0.30%	0.76%	1.22%
	Cycle 3	0.42%	0.83%	1.51%

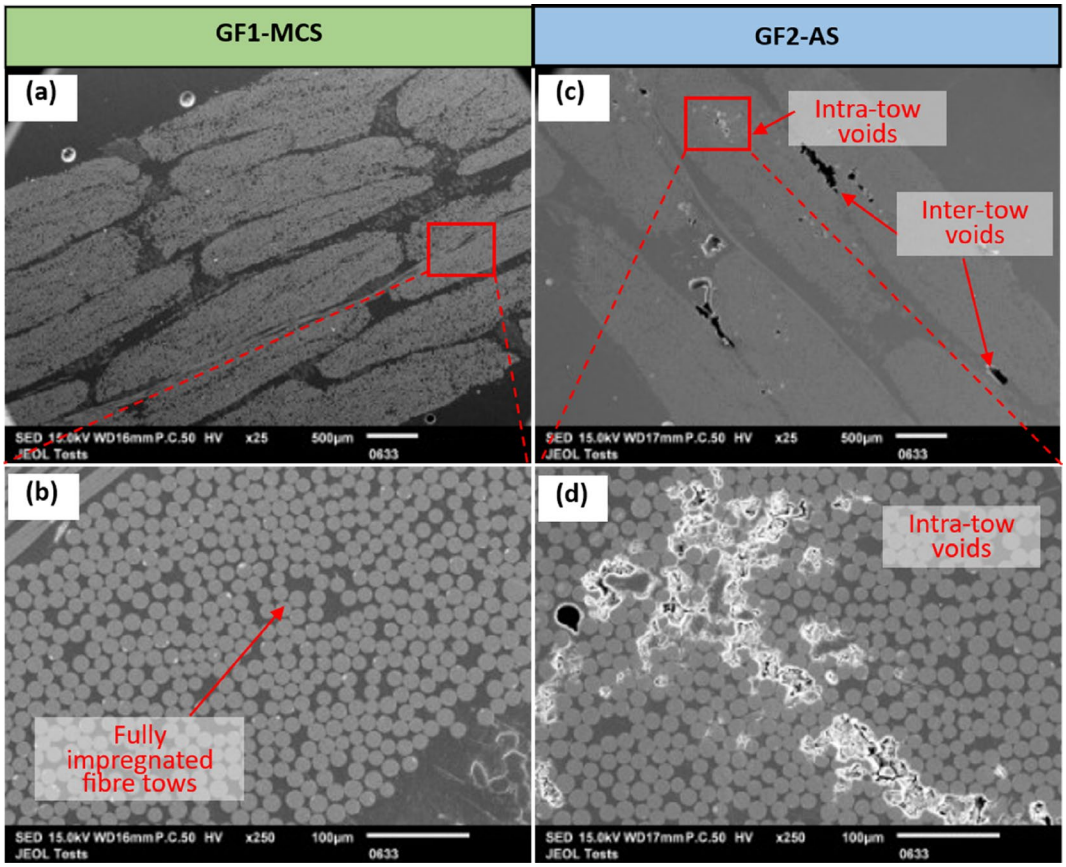

FIGURE 5 | Representative cross-sectional SEM images of acrylic-matrix composites reinforced with: (a) GF1-MCS ×25, (b) GF1-MCS ×250, (c) GF2-AS ×25, (d) GF2-AS ×250. Coupons of the same thickness (for water diffusion measurement) are shown. Inter- and intra-tow voids are present in GF2-AS/acrylic composites, but void content is low in GF1-MCS.

fiber-wetting [25, 26]. GF1-MCS has a tow size of 1200 TEX and a GF diameter of 13 μm compared to GF2-AS, which has a tow size of 2400 TEX and fiber diameter of 16 μm. The larger diameter and tow size mean there are fewer resin flow channels within the fiber tows in the fabric, increasing the likelihood of voids.

3.2.3 | Damage Mechanisms

The increasing diffusion coefficients and final water contents of the cast acrylic and both composites show that all three materials sustained permanent damage during the absorption/drying cycles. In the matrix, this damage may be physical or chemical degradation. Physical degradation occurs due to matrix swelling during absorption and shrinkage during desorption, creating stress concentrations and cracking [27], allowing for easier water penetration for the second absorption cycle. Chemical damage is also possible in acrylic matrices via hydrolysis of the ester side groups [28, 29]. The masses of the cast acrylic coupons and composites were measured during the drying stage, and the average change in weight of the neat resin during the second drying cycle is plotted in Figure 6. After the drying cycle, there was a slight mass decrease of 0.19% which may indicate leaching of unreacted monomer or degradation products from the polymer [28]. Similar decreases of 0.14% and 0.10% after the second drying cycle were measured for GF1-MCS/acrylic and GF2-AS/acrylic, respectively.

Physical damage to the composites via relaxation of the fiber–matrix interface is evaluated by calculating the interfacial free

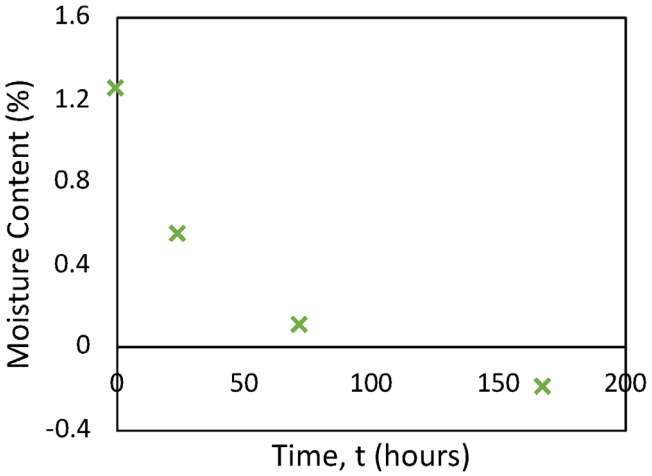

FIGURE 6 | The moisture content of the neat resin coupons vs. the number of hours they were subject to drying conditions during the second drying cycle. A small loss in mass (0.19%) is observed.

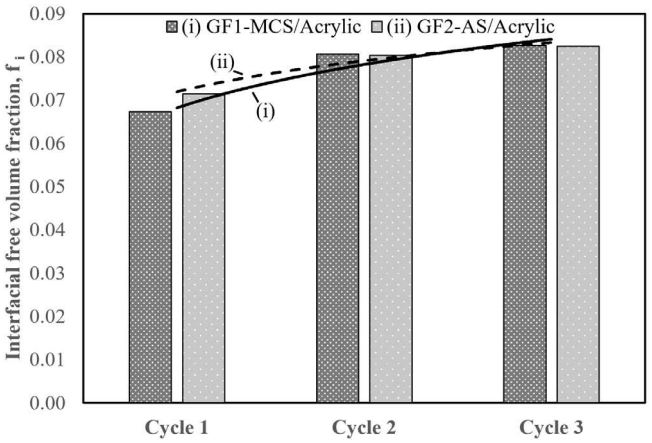

FIGURE 7 | The calculated interfacial free volume fractions of the composites during each absorption cycle. Logarithmic curves of the form $f_i = c \cdot \ln(\text{Cycle}) + d$ are fit to the data for (i) GF1-MCS/acrylic and (ii) GF2-AS/acrylic.

volume fraction during each absorption cycle from Equations (3) and (4). Calculating f_{i0} according to Equation (3), using values from Table 3 for fiber and void contents, gives values of 0.41% and 2.68% for the GF1-MCS and GF2-AS laminates, respectively. From Figure 5, although a portion of the initial void content of GF2-AS (Figure 5c,d) presents as interfacial looseness, the majority appears to be inter-tow voids. It is therefore evident that the assumption of initial void content being equal to f_{i0} does not apply to the present work. Equation (3) therefore overestimates f_{i0} for GF2-AS, and so the values cannot be compared between the two materials.

The interfacial free volume fractions of the GF1-MCS and GF2-AS composites for each immersion cycle are calculated via Equation (4). Values for D_e and D_P were taken from Table 4, and the free volume fraction in the polymer was taken to be $f_p = 0.08$ [13]. The results have been presented in Figure 7, where the interfacial free volume fractions of the materials have been compared across absorption cycles. The increases in f_i observed in both composites can be attributed to the degradation of the fiber matrix interface under cyclic immersion, with the first cycle causing the greatest damage. The values of f_i converged in subsequent cycles as interfacial damage progressed, suggesting similar degrees of interfacial damage between the sizing agents. These increases are found to be logarithmic, and curves of the form $f_i = c \cdot \ln(\text{Cycle}) + d$ are fitted in Figure 7, where c and d are constants, and Cycle refers to the absorption cycle number. The values for c were 0.015 and 0.010, and the values of d were 0.068 and 0.072 for GF1-MCS/acrylic and GF2-AS/acrylic, respectively. This agrees with Tsenoglou et al. [13], where a logarithmic increase in f_i with immersion cycle number was recorded for a GF/polyester composite containing a silane-based sizing agent.

3.3 | Effects of Water Absorption on Quasi-Static Mechanical Properties

3.3.1 | Property Retention

The mechanical properties of GF2-AS/acrylic composites are presented in Table 5 and compared with the results for GF1-MCS/acrylic from [3]. In the dry specimens, GF2-AS/acrylic has a higher modulus but a lower strength than GF1-MCS/acrylic in each test, both fiber- and matrix-dominated.

Comparing the absolute values, however, is complicated by the differences in fiber sizing, fiber diameter, and tow size. While large tow size and large diameter fabrics are generally lower in cost, a smaller fiber diameter is linked to an increased fiber strength, which has been attributed to a lower probability of flaws causing premature failure [30, 31] or differences in the manufacturing (drawing speed, melt temperature, and chemical composition) of the fibers [31, 32]. The fiber modulus is less strongly affected by the diameter, with theoretical modulus values matching measured values much more closely than for strength [33–35]. In addition, a lower fiber diameter increases the surface area available to interact with the matrix. Since GF2-AS has a larger fiber diameter, this could explain the lower strengths but higher moduli of GF2-AS/acrylic in fiber-dominated tests, but not in the matrix-dominated tests.

All else being equal, a larger tow size results in a greater void content, as discussed in Section 3.2.2, and so diffusion of water was faster in GF2-AS/acrylic. When comparing the mechanical tests, however, the GF1-MCS/acrylic coupons were manufactured as part of a different study and therefore have a higher void content than GF2-AS/acrylic—at approximately 2%—despite the latter's larger tow diameter. The lower strengths of GF2-AS/acrylic are therefore not attributed to differences in void content.

Given these differences between the fabrics, comparisons between the percentage retention of mechanical properties are more useful. In general, there is no clear improvement in property retention after water aging by using GF2-AS, as shown in Table 5. The drops in transverse properties (90°) give an indication of the strength of the fiber/matrix interface. The 90° tensile strength of GF1-MCS/acrylic drops by only 4% after water aging compared to an 18% drop in the GF2-AS/acrylic material. Though the 90° flexure strength drops are reversed (−19% for GF2-AS/acrylic vs. −23% for GF1-MCS/acrylic), still GF1-MCS/

acrylic has significantly higher 90° flexure strength than GF2-AS/acrylic before and after water aging. This indicates that the multi-compatible sizing performs better than the tailored sizing agent. The property which shows the largest difference in retention with GF2-AS is the short beam strength, although it should be noted that the dry short beam strength of GF2-AS/acrylic is 19% lower than that of GF1-MCS/acrylic to begin with. After aging, both reinforcements have similar short beam strengths at 39.5 MPa versus 39.0 MPa for GF1-MCS/acrylic and GF2-AS/acrylic, respectively. Short beam strength has a strong reliance on the interface, which may indicate a lower dry interfacial strength in GF2-AS/acrylic.

3.3.2 | Fractography

SEM images of both dry and aged 0° tensile fracture surfaces (using GF2-AS fabric) are presented in Figure 8. As was found in [3], the dry fibers remain bonded to the matrix, which indicates strong interfacial bonding. Shear cusps are present due to a longitudinal splitting failure mode. In the aged specimens, however, the fibers are bare, indicating deterioration of the interfacial bonding. In our previous work using GF1-MCS [3], this deterioration was attributed to hydrolysis of the multi-compatible sizing's agent's silane coupling agent, and from Figure 8 it appears that the same degradation mechanism occurs with the tailored sizing agent of GF2-AS.

3.4 | Effects of Water Absorption on Fatigue

3.4.1 | S–N Curves

S–N curves comparing dry and aged GF2-AS/acrylic specimens are presented in Figure 9, and comparisons between GF2-AS/acrylic and GF1-MCS/acrylic (from [19]) are presented in Figure 10. The values for A and b (Equation 5) from the fitted curves are available in Table 6. All experimental data are provided as points in each graph, and the fitted curve is provided as a solid line between 40% and 80% of the UTS. The UTS of the

TABLE 5 | A comparison between the mechanical properties of GF2-AS/acrylic with previously published results of GF1-MCS/acrylic [3].

		GF2-AS/acrylic			GF1-MCS/acrylic [3]		
Test	**Property**	**Dry**	**Aged**	**% Change**	**Dry**	**Aged**	**% Change**
0° tension	Modulus (GPa)	35.3 ± 3.0	33.4 ± 3.2	−5	33.2 ± 2.2	34.5 ± 2.8	+4
	Strength (MPa)	683 ± 62	541 ± 25	−21	750 ± 61	667 ± 64	−11
90° tension	Modulus (GPa)	10.5 ± 0.7	6.9 ± 1.0	−34	9.3 ± 0.7	8.4 ± 0.4	−10
	Strength (MPa)	37.1 ± 2.2	30.4 ± 1.6	−18	37.1 ± 1.5	35.8 ± 4.5	−4
0° flexure	Modulus (GPa)	36.1 ± 3.6	36.3 ± 3.7	0	31.6 ± 1.6	31.3 ± 0.8	−1
	Strength (MPa)	789 ± 80	706 ± 34	−10	810 ± 40	678 ± 53	−16
90° flexure	Modulus (GPa)	10.6 ± 0.7	8.4 ± 0.7	−21	9.7 ± 0.6	8.0 ± 0.5	−17
	Strength (MPa)	68.3 ± 5.2	55.3 ± 4.1	−19	96.5 ± 8.7	74.4 ± 7.3	−23
Short beam strength	Strength (MPa)	46.6 ± 1.6	39.0 ± 1.6	−16	57.3 ± 0.8	39.4 ± 2.3	−31

Note: The dry properties and change due to water absorption are presented for both composites. Note that the 0° properties have been normalized to 50% FVF for both reinforcements.

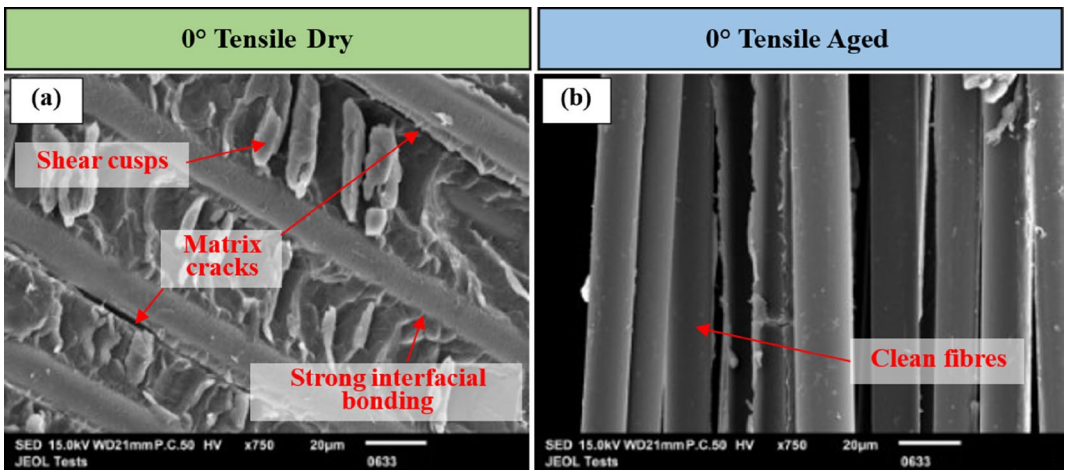

FIGURE 8 | SEM images of the fracture surfaces of (a) dry and (b) aged 0° tensile coupons. Crack propagation through the matrix in (a), instead of along the fiber–matrix interface, indicates strong interfacial bonding. The bare fibers in the aged coupon in (b) suggest that the fiber–matrix interface is weakened.

dry and aged GF2-AS/acrylic coupons for fatigue testing were 710 and 578 MPa, respectively. The 95% confidence intervals of the mean curve are shown as dashed lines.

In Figure 9, water absorption is shown to cause consistent decreases in fatigue life for both GF1-MCS/acrylic and GF2-AS/acrylic. The damage mechanisms discussed in Section 3.2.3 are therefore significant in both low- and high-cycle fatigue.

In contrast, while GF1-MCS/acrylic can be seen to outperform GF2-AS/acrylic in low cycle fatigue in both the dry and aged condition (Figure 10a,b, respectively), the *S–N* curves for both materials converge at a higher number of cycles due to a steeper slope in the GF1-MCS/acrylic curves. Similar convergence was observed by Davies et al. [7, 36] in dry and aged acrylic-matrix composites, and by Shah et al. [37] in dry composites with different flax reinforcements.

The differences in low-cycle fatigue are to be expected due to the higher UTS of GF1-MCS/acrylic, as this region is dominated by fiber fracture and the static properties of the composites [21, 38, 39]. The reasons for the convergence as stress is reduced are less clear, and there are several possible contributing factors. As the stress is reduced and the composite approaches high-cycle behavior, the contribution of static modes of failure reduces and failure is dominated by the matrix and fiber–matrix interface. This is plausible considering that the increased UTS in GF1-MCS/acrylic was attributed to smaller diameter fibers, and their contribution to fatigue life would lessen in high-cycle fatigue. Given that the same matrix was used in both composites, this would indicate that the fatigue performance of each fiber sizing is similar.

Differences in FVF may also contribute, as FVF values greater than approximately 40% have been linked to a decrease in the fatigue exponent *b*, and therefore a steeper slope [37, 40, 41]. This has been attributed to an increased likelihood of fiber–fiber contacts, greater shear stresses at the fiber–matrix interface due to closer fiber packing, and an increase in interfacial area increasing the likelihood of interfacial cracks developing [37, 40]. For a given FVF, a smaller fiber diameter also results in a larger number of fibers and a higher interfacial area—23% higher in GF1-MCS vs. GF2-AS given that the surface area to volume ratio (SA:*V*) of a long fiber with radius *r* is given by $SA:V = {}^{2}/_{r}$. This would increase the probability of fiber-fiber contacts, and result in a greater surface to volume ratio; a combination which

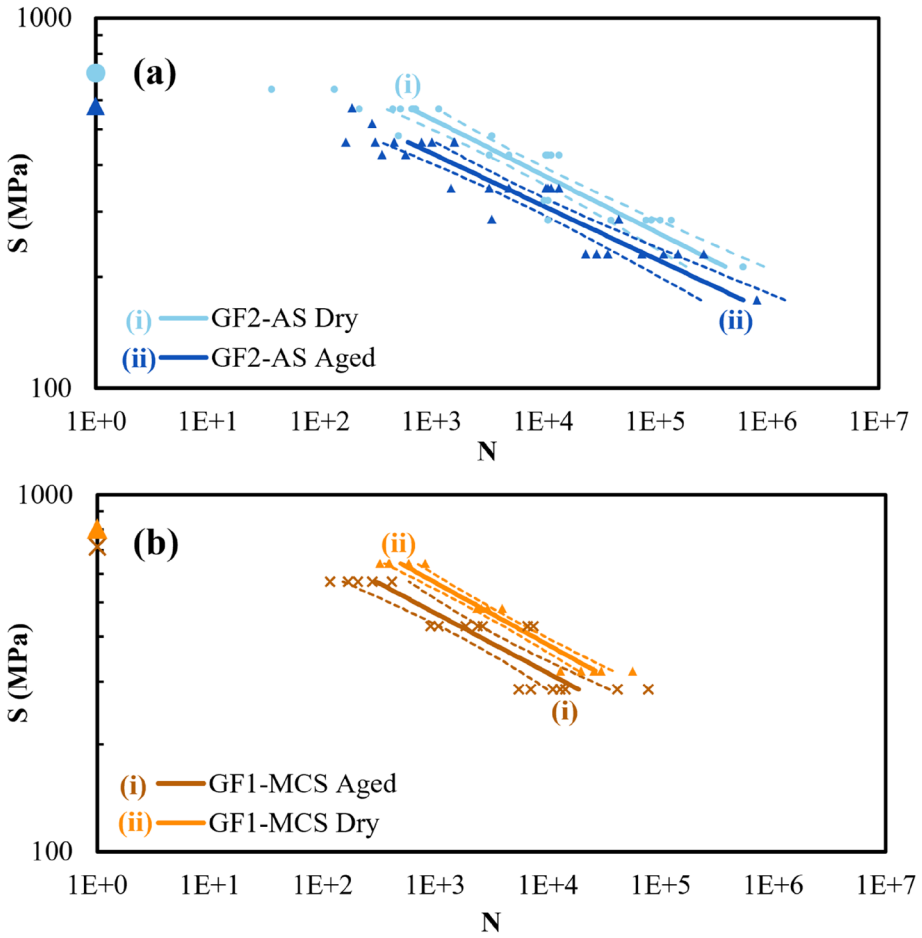

FIGURE 9 | The effect of water absorption on the S–N curves of GF1-MCS/acrylic [19] and GF2-AS/acrylic. The solid lines are the Basquin relation fit to the experimental data for ≤80% of the UTS, and the dashed lines represent the 95% confidence intervals of the mean curve. The mean static UTS at $N = 1$ are included as larger data markers. (a) A comparison of the S–N curves for dry (light blue circles) and aged (dark blue triangles) GF2-AS/acrylic. (b) The same comparison for dry and aged GF1-MCS/acrylic.

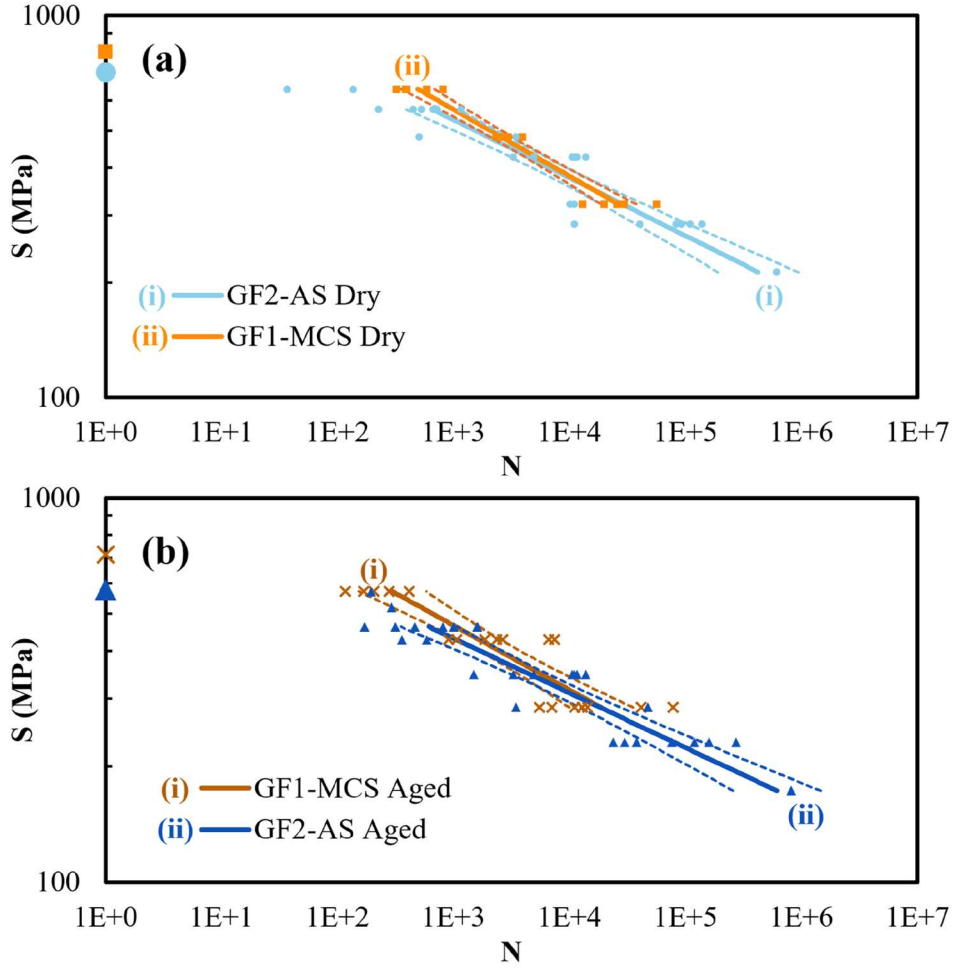

FIGURE 10 | Comparisons between the S–N curves of GF1-MCS/acrylic (from [19]) and GF2-AS/acrylic for (a) dry and (b) saturated coupons. The solid lines are the Basquin relation fit to the experimental data for ≤80% of the UTS, and the dashed lines represent the 95% confidence intervals of the mean curve. The mean static UTS at $N=1$ is included as larger data markers.

TABLE 6 | Basquin coefficients fit to the fatigue data of each material where $\log_{10}N = \log_{10}A + b \cdot \log_{10}S$.

Reinforcement	Condition	*A*	*b*
GF1-MCS [19]	Dry	18.8 [16.8, 20.8]	−5.74 [−6.50, −4.98]
GF1-MCS [19]	Aged	18.9 [15.1, 22.7]	−5.96 [−7.43, −4.49]
GF2-AS	Dry	20.9 [18.0, 23.9]	−6.58 [−7.72, −5.44]
GF2-AS	Aged	21.5 [18.4, 24.6]	−7.02 [−8.26, −5.79]

Note: Data for GF1-MCS/acrylic is taken from [19] and used to fit the Basquin model, rather than the linear combination of exponential functions in the original publication. The 95% confidence intervals on the coefficients are provided in square brackets.

may result in a sharper decline in the GF1-MCS/acrylic S–N curve, similar to the effects observed with a higher FVF.

3.4.2 | Low- and High-Cycle Fatigue

The datapoints outside of the fitted curves (outside the 30%–80% of UTS range) also provide useful information. As seen in Figures 9a(i) and 10a(i), in low-cycle fatigue above ~80% of the UTS, the slopes of the S–N curves begin to decrease. As discussed by Talreja [21, 38, 39], this points to non-progressive fiber breakage being the dominant failure mechanism in this region. Additionally, although only a single datapoint at 30% of UTS was recorded for the dry and aged GF2-AS/acrylic, these datapoints are useful to explore the possibility of a fatigue limit. The data show that, if a fatigue limit exists, it must be lower than 30% of the UTS [41, 42].

3.4.3 | Practical Implications for Material Selection

The fatigue results, in combination with the water absorption behavior and mechanical properties in Sections 3.2 and 3.3, respectively, serve two practical purposes. They allow the performance of GF/acrylic to be benchmarked against more

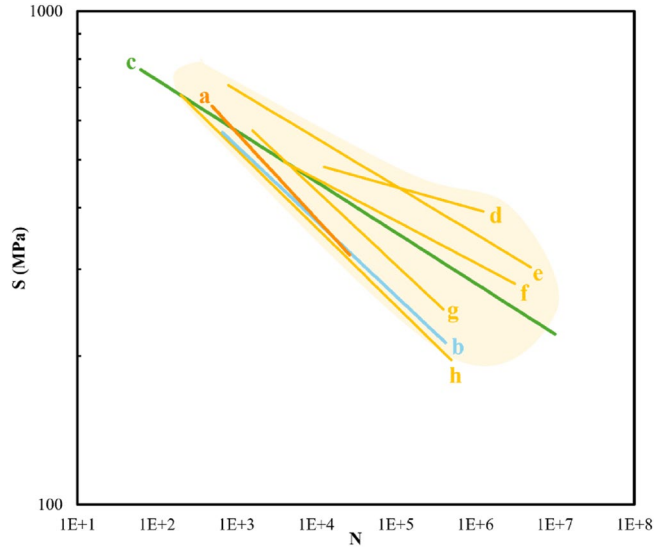

FIGURE 11 | *S–N* curves of various 0° UD E-glass composites tested in tension-tension fatigue ($R=0.1$), with curves of the form of Equation (5) fitted to the data. Curve (a) is dry GF1-MCS/acrylic using data from [19], curve (b) is dry GF2-AS/acrylic from the current study, curve (c) is GF/acrylic from Cousins et al. [22], and curves (d)–(h) are select GF/epoxy data from the SNL/MSU/DOE database [43]. Other stitched UD GF/epoxy *S–N* curves from the database are approximately bounded by the region shaded in yellow.

TABLE 7 | Details of the UD0 GF/epoxy composites from the SNL/MSU/DOE database [43] which are included as curves in Figure 11.

Curve	Material name in database
(d)	UNI-PPG1250-EP5
(e)	UNI-PPG1200-EP1
(f)	UNI-OCV1000-EP1
(g)	UNI-PPG1250-EP1
(h)	UNI-PPG1250-EP9

Note: The curves refer to those in Figure 11, and the other details are taken from the database. The naming convention is Reinforcement Type-Fabric-Matrix, for example, UNI-PPG1250-EP5 is a unidirectional fabric L1200/G50-E07, supplied by PPG Fiber Glass, using epoxy resin EP5. For further details the reader is directed to the database [43].

established alternatives such as GF/epoxy, and they provide insight into the performance of specialized sizing agents.

The fatigue behavior of dry GF1-MCS/acrylic and GF2-AS/acrylic is benchmarked against standard GF/epoxy composites which are used in wind turbine blades in Figure 11, as well as data from GF/acrylic from Cousins et al. [22]. The data is extracted from the SNL/MSU/DOE Composite Material Fatigue Database [43], and *S–N* curves are fitted according to Equation (5). Only a few key GF/epoxy *S–N* curves are explicitly included and detailed in Table 7, but the approximate range of all comparable data for recently tested GF/epoxy (i.e., reinforced with unidirectional stitched 0° E-glass fabric) is shaded in yellow. The performance of the dry GF1-MCS/acrylic and GF2-AS/acrylic materials is comparable with the lower range of GF/epoxy composites in high-cycle fatigue, suggesting they meet the standards required in the wind energy industry.

Curve (c) in Figure 11 is GF/acrylic from Cousins et al. [22], which was reinforced with Johns Manville StarRov 086 (1200 TEX, 16 μm fiber diameter) with a multi-compatible sizing agent. Comparing this material with GF2-AS/acrylic (Johns Manville, 2400 TEX, 16 μm fiber diameter, acrylic-tailored) in Figure 11, curve (b), suggests that a tailored sizing agent does not necessarily result in a superior fatigue response. The superior performance in Cousins et al. [22] compared to GF2-AS/acrylic may be due to a lower void content, which X-ray CT scans suggest is 1.4% versus the 2.4% measured in the current study for GF2-AS/acrylic (Table 3). The fatigue data also highlights that a high UTS and good low-cycle performance does not necessarily imply superior performance in high-cycle fatigue; for example, comparing Figure 11 curves (d) and (e), the former has poorer performance at 10^4 cycles but improved performance at 10^6 cycles.

The relative performance of GF1-MCS and GF2-AS is also of interest, as this will indicate whether there is a need to develop specialized reinforcements for use with acrylic resin. In Section 3.4.1, the superior fatigue performance of GF1-MCS/acrylic in low-cycle fatigue and the subsequent convergence with the *S–N* curve of GF2-AS/acrylic in high-cycle fatigue were discussed. The improved low-cycle fatigue performance was attributed to a smaller fiber diameter and higher FVF in GF1-MCS/acrylic, leading to an increase in UTS. It is also possible, however, that a higher FVF and lower fiber diameter result in poorer fatigue performance. If this is the case, there is a balance to be struck between static and fatigue performance, although since tidal turbine blades are usually designed to maximize stiffness [10], a high FVF is a likely target for manufacturers.

It was also discussed as a possibility in Section 3.4.1 that similar matrix and fiber–matrix interface strengths, as well as a decreasing contribution of UTS to fatigue life at lower stress levels, led to a natural convergence of the GF1-MCS/acrylic and GF2-AS/acrylic *S–N* curves. This would offer a twofold advantage for manufacturers.

Firstly, unless the UTS and high-cycle fatigue performance are of interest for the specific application, the similar performance of lower-cost fabrics with larger fiber and tow diameters compared with more expensive fabric in high cycle fatigue gives a route to cost reduction. In tidal turbine blades, for example, the requirement to design for stiffness results in low fatigue loads, in which GF1-MCS/acrylic and GF2-AS/acrylic had similar performance. A caveat is the possibility that larger tow sizes result in a higher void content (Section 3.1), which may increase the rate of water absorption and property degradation.

Secondly, convergence of the *S–N* curves due to similar performance of the sizing agents in both the dry and aged conditions suggests that manufacturers may not need to procure niche reinforcements with specialized sizing agents. This is reflected in the lack of consistent improvements in dry or aged mechanical properties, and the similarities in water absorption behavior and damage due to the different sizing agents. It would also be consistent with the excellent mechanical properties that can be

obtained with multi-compatible sized reinforcements [2, 3, 44], as well as the recommendations from the manufacturer of Elium acrylic monomer resins to use widely available polyester- or vinylester-compatible sizing agents [12].

Similar findings regarding the effects of the sizing agent on water absorption are available in the literature; for example, studies comparing incompatible and tailored sizing agents show a significant difference in water absorption behavior [13, 45], but comparisons between the performance of multiple sizing agents which are compatible with the matrix—as is the case with GF1-MCS and GF2-AS—do not show such differences [18].

One component of the acrylic-specific sizing agent which has been tailored for acrylic resin is the silane coupling agent. This is achieved by selecting a reactive organic group for compatibility with the free radical polymerization of methacrylate monomers. The bare fibers in Figure 8 suggest that the bond between the matrix and fibers has been weakened, regardless of tailoring for acrylic resin, which can be attributed to the hydrolysis of the silane coupling agent. This mechanism of interfacial degradation has been extensively studied in the literature [46–48]. If silane coupling agent degradation occurs at the bond with the glass, then a tailored reactive organic group may not necessarily improve resistance to hydrothermal degradation over a multi-compatible sizing agent.

The other components of the sizing agent, such as the film former, also play important roles in the interfacial bond strength and water absorption, as the compatibility and reactivity of fiber coatings with the matrix have been shown to affect both strength and water absorption [13, 45], and it therefore remains an important area of research, particularly with the emergence of new matrix systems. Sizing agent formulations are complex and kept as trade secrets by the manufacturers, so it is difficult to come to a generalized conclusion about the role of sizing agents during water absorption. From the perspective of a manufacturer, a tailored sizing guarantees compatibility with the acrylic resin, in contrast with the chemical incompatibility which is possible with multi-compatible sizing agents [15, 17]. The present work suggests, however, that the fact that a sizing is "specialized" or "tailored" does not guarantee superior mechanical properties, water absorption behavior, or fatigue properties.

4 | Conclusions

Significant confusion exists in the literature concerning the effects of specialized sizing agents in glass fiber reinforced acrylic composites. In this study, water absorption behavior and damage mechanisms in glass fiber reinforced acrylic composites, with a multi-compatible (GF1-MCS/acrylic) and an acrylic-specific (GF2-AS/acrylic) fiber sizing, were compared. Additionally, the mechanical properties and fatigue performance of dry and water-saturated GF1-MCS/acrylic and GF2-AS/acrylic were characterized.

Water diffusion was initially driven by the matrix and void contents, but after repeated absorption–desorption cycles, rapid water absorption was caused by interfacial degradation and relaxation. Water absorption data and fractography suggest this degradation was not prevented by the tailored sizing. Degradation in mechanical properties due to water absorption was therefore observed in both GF1-MCS/acrylic and GF2-AS/acrylic, and no consistent improvements were caused by the specialized sizing agent. Differences between the materials' quasi-static mechanical properties are likely due mainly to different fiber properties and fabric architectures.

Similarly, water absorption caused decreased fatigue life across a range of stresses in both GF1-MCS/acrylic and GF2-AS/acrylic. GF1-MCS/acrylic outperformed GF2-AS/acrylic in low-cycle fatigue in the dry and aged condition, but the S-N curves converged in high-cycle fatigue. This would again suggest similar performance of the sizing agents.

There were therefore no consistent improvements to water absorption, interfacial relaxation, mechanical, or fatigue performance due to the acrylic-specific sizing agent. The larger fiber and tow diameters of the GF2-AS mean that it is likely to be more cost-effective for large structures, and the overall similarity between the behavior of GF1-MCS/acrylic and GF2-AS/acrylic, along with comparisons with literature, suggests that the acrylic-tailored sizing agent did not enhance performance. The performance of both dry GF/acrylic composites was comparable to standard GF/epoxies used in wind turbine blades, according to literature comparisons, and large diameter fabrics with readily available multi-compatible sizing agents may therefore be a cost-effective option for manufacturers of acrylic-matrix composites.

Author Contributions

Conchúr M. Ó Brádaigh: funding acquisition, resources, supervision, writing – review and editing, validation, project administration. **Duncan Hornsby:** conceptualization, investigation, writing – original draft, methodology, formal analysis, project administration, data curation, visualization, validation. **Dipa Ray:** supervision, conceptualization, funding acquisition, writing – review and editing, validation, methodology, project administration, resources. **Machar Devine:** conceptualization, investigation, writing – original draft, methodology, validation, visualization, writing – review and editing, software, formal analysis, project administration, data curation.

Acknowledgments

The authors are grateful for funding provided by the EPSRC Centre for Doctoral Training in Wind and Marine Energy Systems (EP/L016680/1). The authors also gratefully acknowledge Arkema GRL, France for the provision of acrylic resin, and Johns Manville and Saertex for the provision of acrylic-tailored glass fiber reinforcements for this research.

Funding

This work was supported by Engineering and Physical Sciences Research Council, EP/L016680/1.

Conflicts of Interest

The authors declare no conflicts of interest.

Data Availability Statement

The data that support the findings of this study are available from the corresponding author upon reasonable request.

References

1. P. Davies, P. Y. Le Gac, and M. Le Gall, "Influence of Sea Water Aging on the Mechanical Behaviour of Acrylic Matrix Composites," *Applied Composite Materials* 24, no. 1 (2016): 97–111, https://doi.org/10.1007/s10443-016-9516-1.

2. W. Obande, D. Mamalis, D. Ray, L. Yang, and C. M. Ó Brádaigh, "Mechanical and Thermomechanical Characterisation of Vacuum-Infused Thermoplastic- and Thermoset-Based Composites," *Materials & Design* 175 (2019): 107828, https://doi.org/10.1016/j.matdes.2019.107828.

3. M. Devine, A. Bajpai, W. Obande, C. M. Ó Brádaigh, and D. Ray, "Seawater Ageing of Thermoplastic Acrylic Hybrid Matrix Composites for Marine Applications," *Composites Part B: Engineering* 263 (2023): 110879, https://doi.org/10.1016/j.compositesb.2023.110879.

4. W. Obande, D. Ray, and C. M. Ó Brádaigh, "Viscoelastic and Drop-Weight Impact Properties of an Acrylic-Matrix Composite and a Conventional Thermoset Composite—A Comparative Study," *Materials Letters* 238 (2019): 38–41, https://doi.org/10.1016/j.matlet.2018.11.137.

5. R. E. Murray, R. Beach, D. Barnes, et al., "Structural Validation of a Thermoplastic Composite Wind Turbine Blade With Comparison to a Thermoset Composite Blade," *Renewable Energy* 164 (2021): 1100–1107, https://doi.org/10.1016/j.renene.2020.10.040.

6. S. K. Bhudolia, P. Perrotey, and S. C. Joshi, "Mode I Fracture Toughness and Fractographic Investigation of Carbon Fibre Composites With Liquid Methylmethacrylate Thermoplastic Matrix," *Composites Part B: Engineering* 134 (2018): 246–253, https://doi.org/10.1016/j.compositesb.2017.09.057.

7. P. Davies and M. Arhant, "Fatigue Behaviour of Acrylic Matrix Composites: Influence of Seawater," *Applied Composite Materials* 26, no. 2 (2018): 507–518, https://doi.org/10.1007/s10443-018-9713-1.

8. R. Murray, D. R. Snowberg, D. S. Berry, et al., *Manufacturing a 9-Meter Thermoplastic Composite Wind Turbine Blade* (American Society for Composites, 2017), https://doi.org/10.12783/asc2017/15166.

9. IRT Jules Verne, ZEBRA Project Achieves Key Milestone With Production of the First Prototype of Its Recyclable Wind Turbine Blade, https://www.irt-jules-verne.fr/wp-content/uploads/zebra-pr-en-vdef.pdf.

10. R. E. Murray, R. Beach, P. Murdy, et al., Structural Characterization of Deployed Thermoplastic and Thermoset Composite Tidal Turbine Blades (2024), https://www.osti.gov/biblio/2336786.

11. J. L. Thomason, "Glass Fibre Sizing: A Review," *Composites Part A: Applied Science and Manufacturing* 127 (2019): 105619, https://doi.org/10.1016/j.compositesa.2019.105619.

12. Arkema, Elium Product Selector (2024), https://www.arkema.com/files/live/sites/shared_arkema/files/downloads/products-documentations/Incubator/ProductSelector_ELIUM_2024.pdf.

13. C. J. Tsenoglou, S. Pavlidou, and C. D. Papaspyrides, "Evaluation of Interfacial Relaxation due to Water Absorption in Fiber–Polymer Composites," *Composites Science and Technology* 66, no. 15 (2006): 2855–2864, https://doi.org/10.1016/j.compscitech.2006.02.022.

14. J. Beguinel, G. Jean-François, L. Frédéric, G. Pierre, and J. Maupetit, "New Continuous Fiber Reinforced Thermoplastic Composites: An Analysis of Interfacial Adhesion From the Micro Scale to the Macro Scale," Presented at the 20th International Conference on Composite Materials, Copenhagen, July 19–24, 2015 (2015).

15. Z. Boufaida, L. Farge, S. André, and Y. Meshaka, "Influence of the Fiber/Matrix Strength on the Mechanical Properties of a Glass Fiber/Thermoplastic-Matrix Plain Weave Fabric Composite," *Composites Part A: Applied Science and Manufacturing* 75 (2015): 28–38, https://doi.org/10.1016/j.compositesa.2015.04.012.

16. Q. Charlier, F. Lortie, P. Gerard, and J.-F. Gerard, "Interfacial Adhesion Between Glass Fibers and Acrylic-Based Matrices as Studied by Micromechanical Testing," 20th International Conference on Composite Materials, Copenhagen (2015).

17. A. K. Sidharth, M. N. Collins, and A. J. Comer, "Impact of Sizing on Fiber-Matrix Interface of Basalt and Glass Fiber Reinforced Infusible Acrylic Thermoplastic and Bio-Epoxy Thermoset Composites," *Materials & Design* 257 (2025): 114516, https://doi.org/10.1016/j.matdes.2025.114516.

18. J. L. Thomason, "The Interface Region in Glass Fibre-Reinforced Epoxy Resin Composites: 2. Water Absorption, Voids and the Interface," *Composites* 26, no. 7 (1995): 477–485, https://doi.org/10.1016/0010-4361(95)96805-G.

19. D. Stankovic, W. Obande, M. Devine, A. Bajpai, C. M. Ó Brádaigh, and D. Ray, "Accelerated Seawater Ageing and Fatigue Performance of Glass Fibre Reinforced Thermoplastic Composites for Marine and Tidal Energy Applications," *Composites Part C: Open Access* 14 (2024): 100470, https://doi.org/10.1016/j.jcomc.2024.100470.

20. N. Siddgonde, J. A. Quinn, C. M. Ó Brádaigh, and D. Ray, "Mode I Fracture Toughness and Compressive Properties of Glass Fibre Reinforced Acrylic Matrix Composites Before and After Seawater Ageing," *Polymer Composites* 47, no. 12 (2026): 11444–11455, https://doi.org/10.1002/pc.71033.

21. R. Talreja, "Fatigue of Composite Materials: Damage Mechanisms and Fatigue-Life Diagrams," *Proceedings of the Royal Society of London. Series A: Mathematical and Physical Sciences* 378, no. 1775 (1981): 461–475, https://doi.org/10.1098/rspa.1981.0163.

22. D. S. Cousins, Z. Arwood, S. Young, et al., "Infusible Thermoplastic Composites for Wind Turbine Blade Manufacturing: Fatigue Life of Thermoplastic Laminates Under Ambient and Low-Temperature Conditions," *Advanced Engineering Materials* 25, no. 11 (2023): 202201941, https://doi.org/10.1002/adem.202201941.

23. P. Alam, C. Robert, and C. M. Ó Brádaigh, "Tidal Turbine Blade Composites—A Review on the Effects of Hygrothermal Aging on the Properties of CFRP," *Composites Part B: Engineering* 149 (2018): 248–259, https://doi.org/10.1016/j.compositesb.2018.05.003.

24. M. Woo and M. R. Piggott, "Water Absorption of Resins and Composites: IV. Water Transport in Fiber Reinforced Plastics," *Journal of Composites Technology & Research* 10, no. 1 (1988): 20–24, https://doi.org/10.1520/CTR10271J.

25. H. Jinlian, L. Yi, and S. Xueming, "Study on Void Formation in Multi-Layer Woven Fabrics," *Composites Part A: Applied Science and Manufacturing* 35, no. 5 (2004): 595–603, https://doi.org/10.1016/j.compositesa.2003.11.007.

26. G.-W. Lee and K.-J. Lee, "Mechanism of Void Formation in Composite Processing With Woven Fabrics," *Polymers and Polymer Composites* 11, no. 7 (2003): 563–572, https://doi.org/10.1177/096739110301100706.

27. F. Awaja, S. Zhang, M. Tripathi, A. Nikiforov, and N. Pugno, "Cracks, Microcracks and Fracture in Polymer Structures: Formation, Detection, Autonomic Repair," *Progress in Materials Science* 83 (2016): 536–573, https://doi.org/10.1016/j.pmatsci.2016.07.007.

28. H. Bel Haj Frej, R. Léger, D. Perrin, and P. Ienny, "A Novel Thermoplastic Composite for Marine Applications: Comparison of the Effects of Aging on Mechanical Properties and Diffusion Mechanisms," *Applied Composite Materials* 28 (2021): 899–922, https://doi.org/10.1007/s10443-021-09903-0.

29. L. S. A. Smith and V. Schmitz, "The Effect of Water on the Glass Transition Temperature of Poly(Methyl Methacrylate)," *Polymer* 29, no. 10 (1988): 1871–1878, https://doi.org/10.1016/0032-3861(88)90405-3.

30. A. A. Griffith and G. I. Taylor, "VI. The Phenomena of Rupture and Flow in Solids," *Philosophical Transactions of the Royal Society of London. Series A, Containing Papers of a Mathematical or Physical*

Character 221, no. 582–593 (1921): 163–198, https://doi.org/10.1098/rsta.1921.0006.

31. P. K. Gupta, "Strength of Glass Fibers," in *Fiber Fracture*, ed. M. Elices and J. Llorca (Elsevier Science Ltd, 2002), 127–153.

32. W. H. Otto, "Relationship of Tensile Strength of Glass Fibers to Diameter," *Journal of the American Ceramic Society* 38, no. 3 (1955): 122–125, https://doi.org/10.1111/j.1151-2916.1955.tb14588.x.

33. J. L. Thomason, "The Influence of Fibre Length, Diameter and Concentration on the Modulus of Glass Fibre Reinforced Polyamide 6,6," *Composites Part A: Applied Science and Manufacturing* 39, no. 11 (2008): 1732–1738, https://doi.org/10.1016/j.compositesa.2008.08.001.

34. R. Kumar, L. P. Mikkelsen, H. Lilholt, and B. Madsen, "Understanding the Mechanical Response of Glass and Carbon Fibres: Stress-Strain Analysis and Modulus Determination," *IOP Conference Series: Materials Science and Engineering* 942, no. 1 (2020): 12033, https://doi.org/10.1088/1757-899X/942/1/012033.

35. H. Li, "Strength of Glass and Glass Fibers," in *76th Conference on Glass Problems, Ceramic Engineering and Science Proceedings* (The American Ceramic Society, 2016), 1–15.

36. P. Davies, M. Arhant, and E. Grossmann, "Seawater Ageing of Infused Flax Fibre Reinforced Acrylic Composites," *Composites Part C: Open Access* 8 (2022): 100246, https://doi.org/10.1016/j.jcomc.2022.100246.

37. D. U. Shah, P. J. Schubel, M. J. Clifford, and P. Licence, "Fatigue Life Evaluation of Aligned Plant Fibre Composites Through S–N Curves and Constant-Life Diagrams," *Composites Science and Technology* 74 (2013): 139–149, https://doi.org/10.1016/j.compscitech.2012.10.015.

38. E. K. Gamstedt and R. Talreja, "Fatigue Damage Mechanisms in Unidirectional Carbon-Fibre-Reinforced Plastics," *Journal of Materials Science* 34, no. 11 (1999): 2535–2546, https://doi.org/10.1023/A:1004684228765.

39. R. Talreja, "Fatigue of Composite Materials," in *Modern Trends in Composite Laminates Mechanics*, ed. H. Altenbach and W. Becker (Springer Vienna, 2003), 281–294.

40. J. F. Mandell, D. D. Samborsky, and H. J. Sutherland, Effects of Materials Parameters and Design Details on the Fatigue of Composite Materials for Wind Turbine Blades (1999), https://www.osti.gov/biblio/4194.

41. R. P. L. Nijssen, "Fatigue Life Prediction and Strength Degradation of Wind Turbine Rotor Blade Composites," Contractor Report SAND2006-7810P (Sandia National Laboratories, Albuquerque, NM) (2006), https://www.montana.edu/composites/documents/Rogier%20Nijssen%20067810P.pdf.

42. A. D'Amore and L. Grassia, "Principal Features of Fatigue and Residual Strength of Composite Materials Subjected to Constant Amplitude (CA) Loading," *Materials* 12, no. 16 (2019): 12162586, https://doi.org/10.3390/ma12162586.

43. SNL/MSU/DOE Composite Material Fatigue Database, https://energy.sandia.gov/programs/renewable-energy/wind-power/rotor-innovation/rotor-reliability/mhk-materials-database/.

44. W. Obande, C. M. Ó Brádaigh, and D. Ray, "Continuous Fibre-Reinforced Thermoplastic Acrylic-Matrix Composites Prepared by Liquid Resin Infusion—A Review," *Composites Part B: Engineering* 215 (2021): 108771, https://doi.org/10.1016/j.compositesb.2021.108771.

45. R. L. Gorowara, "Interphase formation and environmental degradation in glass fiber/vinyl ester composites" (PhD, University of Delaware, Delaware, 3025805) (2002), https://ui.adsabs.harvard.edu/abs/2002PhDT.30G/abstract.

46. H. Ishida and J. L. Koenig, "A Fourier-Transform Infrared Spectroscopic Study of the Hydrolytic Stability of Silane Coupling Agents on E-Glass Fibers," *Journal of Polymer Science Polymer Physics Edition* 18, no. 9 (1980): 1931–1943, https://doi.org/10.1002/pol.1980.180180906.

47. H. Ishida and J. L. Koenig, "The Reinforcement Mechanism of Fiber-Glass Reinforced Plastics Under Wet Conditions: A Review," *Polymer Engineering & Science* 18, no. 2 (1978): 128–145, https://doi.org/10.1002/pen.760180211.

48. O. Ishai, "Environmental Effects on Deformation, Strength, and Degradation of Unidirectional Glass-Fiber Reinforced Plastics. II. Experimental Study," *Polymer Engineering & Science* 15, no. 7 (1975): 491–499, https://doi.org/10.1002/pen.760150704.

Supporting Information

Additional supporting information can be found online in the Supporting Information section. **Figure S1:** Moisture content vs. the square root of time for the three absorption cycles of neat acrylic (blue), GF2-AS/acrylic (orange) and GF1-MCS/acrylic (green). Each datapoint is the average of 10 specimens. **Figure S2:** Representative stress–strain curves for dry and aged 0° tensile coupons. **Figure S3:** Representative stress–strain curves for dry and aged 90° tensile coupons. **Figure S4:** Representative stress–strain curves for 0° flexure coupons. **Figure S5:** Representative stress–strain curves for 90° flexure coupons. **Figure S6:** Representative stress–strain curves for short beam strength coupons.